Keceli and Kubo, http://www.jgp.org/cgi/content/full/jgp.201411166/DC1

Details of the statistical analyses

Fig. 2 B: Statistical analyses of the voltage-induced activation time constants for WT and WT–WT–WT. We analyzed the time constants of WT and WT–WT–WT by two-factor ANOVA (construct: WT and WT–WT–WT; [ATP]: 3, 10, 30, 100, 300, and 1,000 µM). ANOVA revealed a significant main effect of [ATP] ($F(5,110) = 48.4$; $P < 0.05$). There was no significant main effect of construct ($F(1,110) = 1.5$; $P > 0.05$), and there was no significant interaction ($F(5,110) = 0.4$; $P > 0.05$). The results showed that activation time constants of WT–WT–WT were similar to WT protomer at identical [ATP].

Figs. 2 B and S4 B: Statistical analyses of the voltage-induced activation time constants for WT–WT–WT and TTCs with one K308A. Time constants at −160 mV at various [ATP] compared for the WT–WT–WT and TTCs with one K308A mutation (Figs. 2 B and S4 B) using two-factor ANOVA (construct: WT–WT–WT, K308A–WT–WT, WT–K308A–WT, and WT–WT–K308A; [ATP]: 10, 30, 100, 300, and 1,000 µM). ANOVA revealed a significant main effect of [ATP] ($F(4,324) = 106.4$; $P < 0.05$). There was no significant main effect of construct ($F(3,324) = 1.8$; $P > 0.05$), and there was no significant interaction ($F(12,324) = 1.8$; $P > 0.05$). The results showed that activation time constants at identical [ATP] for WT–WT–WT and TTCs with one K308A were similar. In summary, voltage-induced activation time constants calculated from fittings of the voltage-induced activation phases with a single-exponential function at various [ATP] and membrane potentials were highly similar in all these constructs (Figs. 2 B and S4 B).

Fig. 2 (D–F): Statistical analyses of the EC_{50} and Hill coefficients for WT, WT–WT–WT, and TTCs with one K308A. EC_{50} and Hill values for WT and WT–WT–WT (Fig. 3 E) were compared using nonparametric *t* tests (Mann–Whitney U test). EC_{50} and Hill values for WT and WT–WT–WT were not significantly different (EC_{50}, $U = 42.0$, $P > 0.05$; Hill, $U = 70$, $P > 0.05$). EC_{50} and Hill values of the TTCs were analyzed by one-factor nonparametric ANOVAs (Kruskal–Wallis test). The ANOVA statistic was significant ($H = 10.2$ (3; $n = 38$); $P < 0.05$), which indicates that the EC_{50} value of at least one of the tandem constructs was different from at least one of the others. Pairwise comparisons performed using Dunn's post-test showed that only the WT–WT–WT versus K308A–WT–WT pair had significantly different EC_{50} values ($P < 0.05$). The outcome of the ANOVA revealed that Hill values of the tandem constructs were not significantly different ($H = 3.7$ (3; $n = 38$); $P > 0.05$).

Fig. S4 D: Statistical analyses of the $V_{1/2}$ (mV) or Z values of WT, WT–WT–WT, and TTCs with one K308A mutation. $V_{1/2}$ (mV) or Z values of WT, WT–WT–WT, and TTCs with one K308A mutation (Fig. S4 D) were analyzed using one-factor ANOVAs (construct: WT, WT–WT–WT, K308A–WT–WT, WT–K308A–WT, and WT–WT–K308A). ANOVAs revealed that there was no significant effect of construct on $V_{1/2}$ (mV) or Z values ($V_{1/2}$: $F(4, 28) = 0.24$, $P > 0.05$; Z: $F(4, 28) = 0.50$, $P > 0.05$).

Fig. 5 C: Statistical analyses of the conductance ratios at −60 and −160 mV for TTCs harboring various numbers of T339S. The ratios of conductance at −60 to −160 mV for the TTCs T339S–T339S–T339S, WT–T339S–T339S, WT–T339S–WT, and WT–WT–WT were compared by one-factor ANOVA and post-hoc Fisher's least significant difference tests. ANOVA revealed a significant effect of the number of T339S mutation in the TTCs ($F(3,26) = 43.0$; $P < 0.05$). Multiple comparisons showed that as the number of T339S mutation decreased, the conductance ratios of the TTCs decreased gradually.

Fig. 5 E: Statistical analyses of the voltage-induced activation time constants for TTCs harboring various numbers of T339S. The time constants measured by single-exponential fitting of the voltage-induced activation traces showed a gradual acceleration in gating as the number of T339S mutations in the trimer increased (Fig. 5, D and E). The time constants for the TTCs (WT–T339S–T339S, WT–T339S–WT, and WT–WT–WT) were compared by one-factor ANOVA and post-hoc Fisher's LSD tests. ANOVA revealed a significant effect on the number of T339S mutations in the TTC ($F(2,58) = 31.0$; $P < 0.05$). Multiple comparisons showed that there was a gradual acceleration in gating as the number of T339S mutations in the trimer increased.

Fig. 6 (C and D): Statistical analyses of the voltage-induced activation time constants for K308A–D315A–WT and WT–K308A&D315A–WT. Voltage-induced activation time constants at −160 mV for various [ATP] were compared for the K308A–D315A–WT and WT–K308A&D315A–WT using two-factor ANOVA (construct: K308A–D315A–WT and WT–K308A&D315A–WT; [ATP]: 3, 10, 30, 100, 300, and 1,000 µM). ANOVA revealed significant main effects of [ATP] ($F(5, 154) = 31.1$; $P < 0.05$) and construct ($F(1,154) = 75.7$; $P < 0.05$), and a significant interaction ($F(5, 154) = 10.2$; $P < 0.05$). The results showed that the activation time constants of *cis* configuration were different from the *trans* configuration. Furthermore, the effect of increasing [ATP] on the voltage-induced activation speed of the *cis* construct was different from the *trans* construct.

Fig. 6 (G and H): Statistical analyses of the $V_{1/2}$ (mV) or Z values for K308A–D315A–WT and WT–K308A&D315A–WT. $V_{1/2}$ (mV) values of K308A–D315A–WT and WT–

K308A&D315A–WT (Fig. 6 G) at various [ATP] were analyzed by two-factor ANOVA (construct: K308A–D315A–WT and WT–K308A&D315A–WT; [ATP]: 3, 10, 30, 100, 300, and 1,000 μM). ANOVA revealed significant main effects of construct ($F(1, 71) = 11.9$; $P < 0.05$) and [ATP] ($F(5, 71) = 2.4$; $P < 0.05$), and a significant interaction ($F(5, 71) = 3.3$; $P < 0.05$). The effect of TTCs was further analyzed using Fisher's LSD multiple comparisons. For all [ATP] except for 10 μM, $V_{1/2}$ (mV) values of K308A–D315A–WT and WT–K308A&D315A–WT were significantly different ($P < 0.05$). The results showed that the [ATP] effect on calculated $V_{1/2}$ (mV) values from the G-V relationship was different between the *cis* and *trans* configurations. Z values of K308A–D315A–WT and WT–K308A&D315A–WT at various [ATP] (Fig. 6 H) were analyzed by two-factor ANOVA (construct: K308A–D315A–WT and WT–K308A&D315A–WT; [ATP]: 3, 10, 30, 100, 300, and 1,000 μM). ANOVA revealed a significant main effect of ATP ($F(5, 71) = 3.5$; $P < 0.05$). There was no significant effect of construct ($F(1, 71) = 0.2$; $P > 0.05$), and there was no significant interaction ($F(5, 71) = 1.8$; $P > 0.05$). The results showed that Z values for the *cis* and *trans* configurations for these two TTCs were similar.

Fig. 7 B: Statistical analyses of the voltage-induced activation time constants for D315A&K69A–WT–WT and WT–D315A–K69A. Voltage-induced activation time constants at −160 mV for various [ATP] were compared for the D315A&K69A–WT–WT and WT–D315A–K69A using two-factor ANOVA (construct: D315A&K69A–WT–WT and WT–D315A–K69A; [ATP]: 3, 10, 30, 100, 300, and 1,000 μM). ANOVA revealed significant main effects of [ATP] ($F(5, 87) = 97.8$; $P < 0.05$) and construct ($F(1,87) = 4.1$; $P < 0.05$), and a significant interaction ($F(5, 87) = 62.9$; $P < 0.05$). The results showed that the activation time constants of the two TTCs with different configurations were not similar. Furthermore, the effect of increasing [ATP] on the voltage-induced activation speed of the two configurations was also different.

Fig. 7 D: Statistical analyses of the $V_{1/2}$ (mV) or Z values for D315A&K69A–WT–WT and WT–D315A–K69A. $V_{1/2}$ (mV) values of D315A&K69A–WT–WT and WT–D315A–K69A at various [ATP] (Fig. 7 D) were analyzed by two-factor ANOVA (construct: D315A&K69A–WT–WT and WT–D315A–K69A; [ATP]: 3, 10, 30, 100, and 300 μM). ANOVA revealed a significant main effect of construct ($F(1, 62) = 37.7$; $P < 0.05$) and a significant interaction ($F(4, 62) = 3.0$; $P < 0.05$). There was no significant effect of [ATP] ($F(4, 62) = 0.6$; $P > 0.05$). The effect of TTC was further analyzed using Fisher's LSD multiple comparisons. For all [ATP] except 3 μM, $V_{1/2}$ (mV) values of D315A&K69A–WT–WT and WT–D315A–K69A were significantly different ($P < 0.05$). The results also showed that the effect of an increase in [ATP] on calculated $V_{1/2}$ (mV) values from the G-V relationship was different between the two configurations. Z values of D315A&K69A–WT–WT and WT–D315A–K69A at various [ATP] (Fig. 7 D) were analyzed by two-factor ANOVA (construct: D315A&K69A–WT–WT and WT–D315A–K69A; [ATP]: 3, 10, 30, 100, and 300 μM). ANOVA revealed significant main effects of construct ($F(1, 62) = 40.9$; $P < 0.05$) and [ATP] ($F(4, 62) = 7.6$; $P < 0.05$), and a significant interaction ($F(4, 62) = 3.5$; $P < 0.05$). The results showed that the effect of an increase in [ATP] was different between these two constructs.

Fig. 8 (C and D): Statistical analyses of the voltage-induced activation time constants for K308A–T339S–WT and WT–K308A&T339S–WT. Voltage-induced activation time constants at −160 mV for various [ATP] were compared for the K308A–T339S–WT and WT–K308A&T339S–WT (Fig. 8, C and D) using two-factor ANOVA (construct: K308A–T339S–WT and WT–K308A&T339S–WT; [ATP]: 3, 10, 30, 100, 300, and 1,000 μM). ANOVA revealed a significant main effect of [ATP] ($F(5, 115) = 217.0$; $P < 0.05$) and a significant interaction ($F(5, 115) = 10.4$; $P < 0.05$). There was no significant main effect of TTC ($F(1, 115) = 0.1$; $P > 0.05$). The results showed that the *cis* and *trans* configurations have similar activation time constants, but there was also a slight but statistically significant difference between the effect of the increase in [ATP] on the speed of the voltage-induced activation phase between the two constructs.

Fig. 8 (G and H): Statistical analyses of the $V_{1/2}$ (mV) or Z values for K308A–T339S–WT and WT–K308A&T339S–WT. $V_{1/2}$ (mV) values of K308A–T339S–WT and WT–K308A&T339S–WT at various [ATP] (Fig. 8 G) were analyzed by two-factor ANOVA (construct: K308A–T339S–WT and WT–K308A&T339S–WT; [ATP]: 3, 10, 30, 100, 300, 1,000, and 3,000 μM). ANOVA revealed a significant main effect of ATP ($F(6, 92) = 9.0$; $P < 0.05$). There was no significant main effect of TTC ($F(1, 92) = 0.1$; $P > 0.05$), and there was no significant interaction ($F(6, 92) = 0.6$; $P > 0.05$). The results showed that the effect of [ATP] on $V_{1/2}$ (mV) values of K308A–T339S–WT and WT–K308A&T339S–WT were similar. Z values of K308A–T339S–WT and WT–K308A&T339S–WT at various [ATP] (Fig. 8 H) were analyzed by two-factor ANOVA (construct: K308A–T339S–WT and WT–K308A&T339S–WT; [ATP]: 3, 10, 30, 100, 300, 1,000, and 3,000 μM). ANOVA revealed a significant main effect of ATP ($F(6, 92) = 3.5$; $P < 0.05$) and a significant interaction ($F(6, 92) = 2.9$; $P < 0.05$). There was no significant main effect of TTC ($F(1, 92) = 3.4$; $P > 0.05$). The results showed that Z values of the two constructs were highly similar.

Fig. 9 (C and D): Statistical analyses of the voltage-induced activation time constants for D315A–T339S–WT and WT–D315A&T339S–WT. Voltage-induced activation time constants at −160 mV for various [ATP] were compared for the D315A–T339S–WT and WT–D315A&T339S–WT (Fig. 9, C and D) using two-factor ANOVA (construct: D315A–T339S–WT and WT–D315A&T339S–WT;

[ATP]: 3, 10, 30, 100, 300, and 1,000 µM). ANOVA revealed a significant main effect of [ATP] ($F(5, 144) = 163.0$; $P < 0.05$). There was no significant main effect of TTC ($F(1,144) = 0.1$; $P > 0.05$) or significant interaction ($F(5,144) = 0.2$; $P > 0.05$). The results showed that both activation time constants of constructs and the effect of increase in [ATP] were highly similar.

Fig. 9 (G and H): Statistical analyses of the $V_{1/2}$ (mV) or Z values for D315A–T339S–WT and WT–D315A&T339S–WT. $V_{1/2}$ (mV) values of D315A–T339S–WT and WT–D315A&T339S–WT at various [ATP] (Fig. 9 G) were analyzed by two-factor ANOVA (construct: D315A–T339S–WT and WT–D315A&T339S–WT; [ATP]: 3, 10, 30, 100, 300, and 1,000 µM). ANOVA revealed a significant main effect of ATP ($F(5, 86) = 5.5$; $P < 0.05$). There was no significant main effect of TTC ($F(1, 86) = 0.1$; $P > 0.05$) or significant interaction ($F(5, 86) = 0.3$; $P > 0.05$). The results showed that an increase in [ATP] effect on $V_{1/2}$ (mV) values of D315A–T339S–WT and WT–D315A&T339S–WT was highly similar.

Z values of D315A–T339S–WT and WT–D315A&T339S–WT at various [ATP] (Fig. 9 H) were analyzed by two-factor ANOVA (construct: D315A–T339S–WT and WT–D315A&T339S–WT; [ATP]: 3, 10, 30, 100, 300, and 1,000 µM). ANOVA revealed a significant main effect of ATP ($F(5, 86) = 6.3$; $P < 0.05$). There was no significant main effect of TTC ($F(1, 86) = 1.2$; $P > 0.05$) or significant interaction ($F(5, 86) = 0.2$; $P > 0.05$). The results showed that an increase in [ATP] effect on Z values of D315A–T339S–WT and WT–D315A&T339S–WT was highly similar.

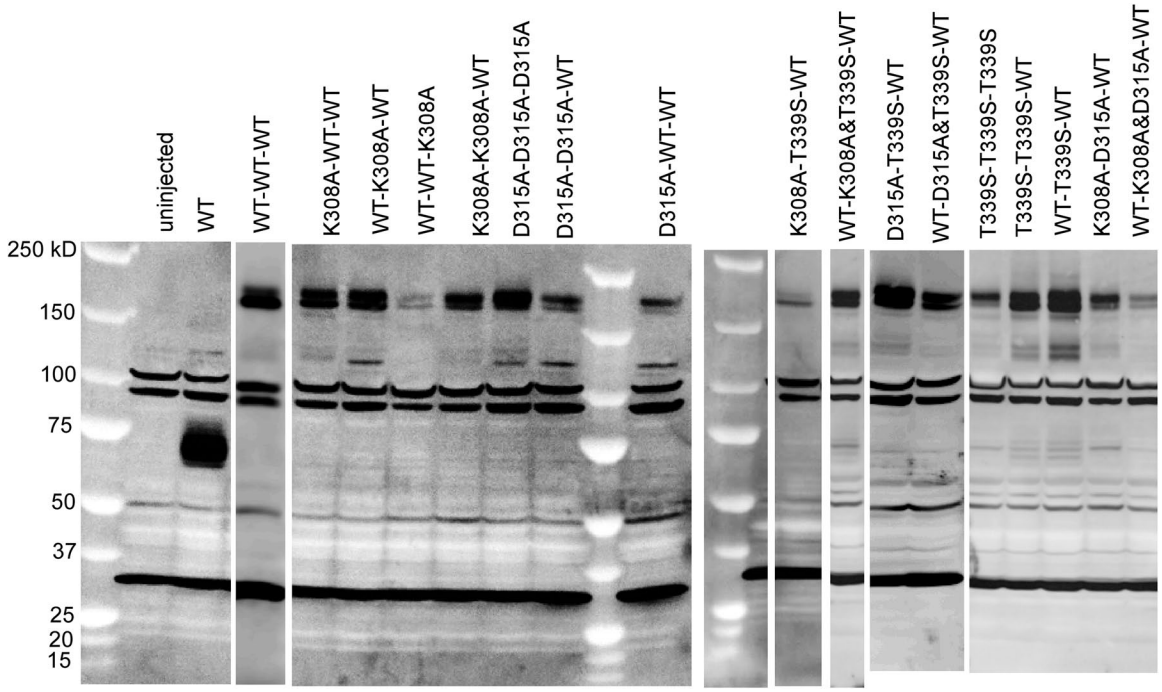

Figure S1. Western blotting of the protein constructs used in the experiments. Details of Western blotting are given in Materials and methods. Expressions of three tandem repeat protein of ∼170 kD were confirmed for all constructs. The dual bands could be caused by posttranslational modifications.

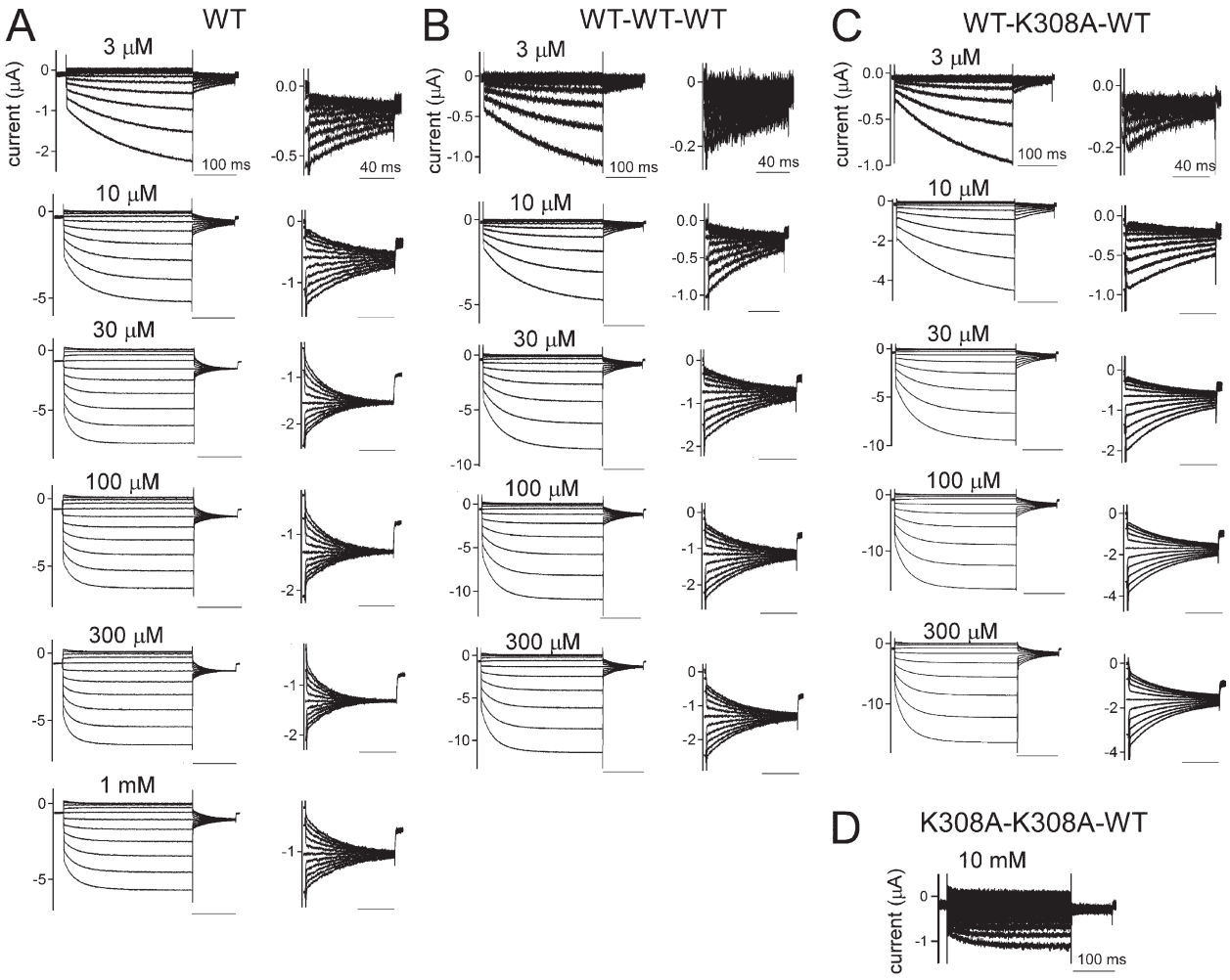

Figure S2. Representative macroscopic current recordings of WT (A), WT–WT–WT (B), WT–K308A–WT (C), and K308A–K308A–WT (D) constructs. Responses were evoked by step pulses from 40 to −160 mV in 20-mV decrements from the holding potential of −40 mV in the steady state after the application of various [ATP]. Tail currents were recorded at −60 mV, and their enlarged images are shown next to the main activation traces. A set of responses for each construct was recorded from the same oocytes at various [ATP].

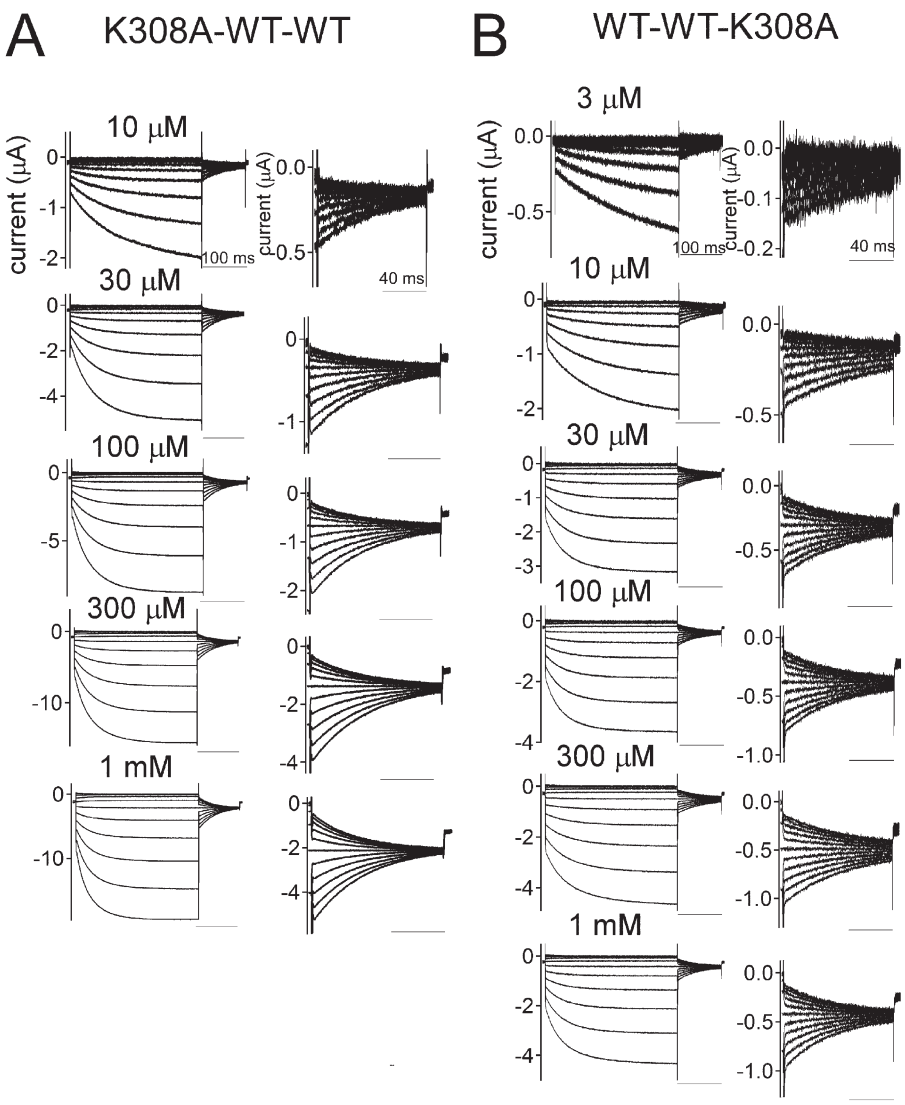

Figure S3. Two ATP-binding sites are necessary and sufficient for voltage- and [ATP]-dependent gating of $P2X_2$. (A and B) Representative macroscopic recordings of K308A–WT–WT (A) and WT–WT–K308A (B), with pulse protocol. Step pulses from 40 to −160 mV were applied in 20-mV decrements. The holding potential was −40 mV. Tail currents were recorded at −60 mV, and their enlarged images are shown next to the main activation traces.

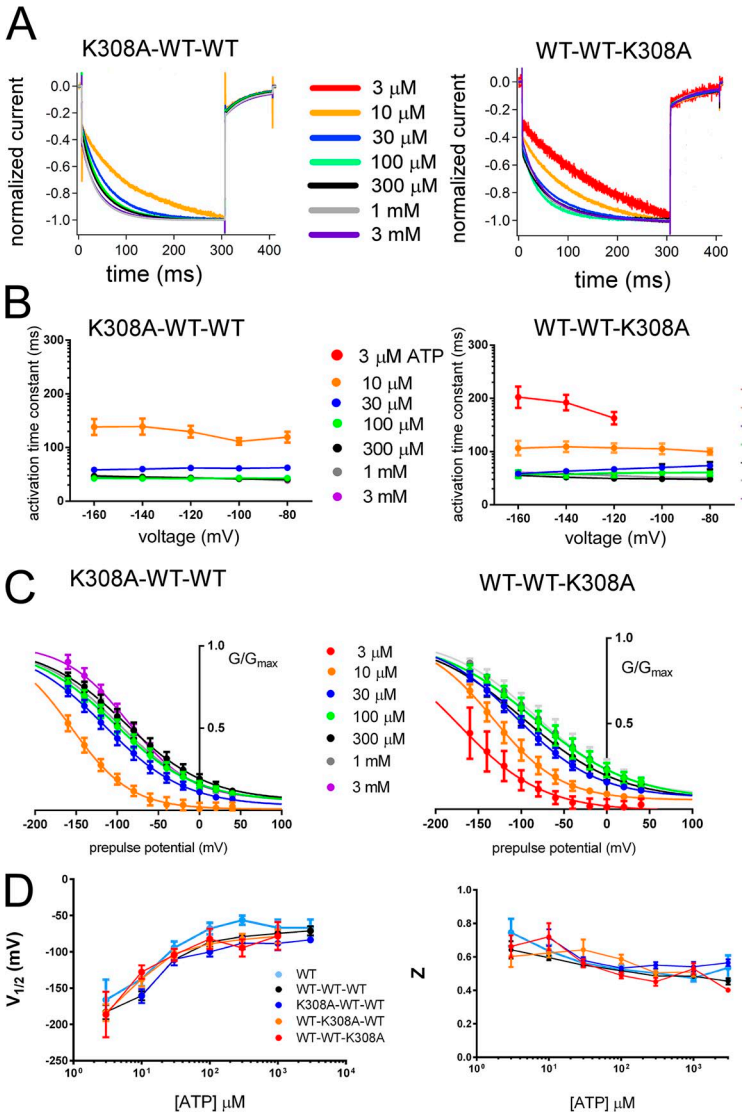

Figure S4. One K308A mutation in the ATP-binding site does not have a position effect for voltage- and [ATP]-dependent gating. Analysis of K308A–WT–WT and WT–WT–K308A shows similar voltage- and [ATP]-dependent gating to that observed in WT–K308A–WT (Fig. 3). (A) Normalized voltage-induced activation traces at −160 mV for K308A–WT–WT (left) and WT–WT–K308A (right) at various [ATP] from the representative data shown in Fig. S3. (B) Dependence of the activation kinetics on voltage and [ATP] for K308A–WT–WT (left) and WT–WT–K308A (right). Mean (± SEM) activation time constants for K308A–WT–WT (n = 10–17) and WT–WT–K308A (n = 13–15) at various [ATP] and membrane potentials are shown. (C) Mean (± SEM) normalized G-V relationships at various [ATP] for tandem trimers K308A–WT–WT (left; n = 7) and WT–WT–K308A (right; n = 6) derived from the maximum tail current responses by fitting with the two-state Boltzmann equation as described in Materials and methods. (D) Mean (± SEM) $V_{1/2}$ (mV) and Z values derived from the Boltzmann fitting of the maximum tail currents at −60 mV for K308A–WT–WT (n = 7) and WT–WT–K308A (n = 6) are represented for various [ATP] together with WT and WT–WT–WT.

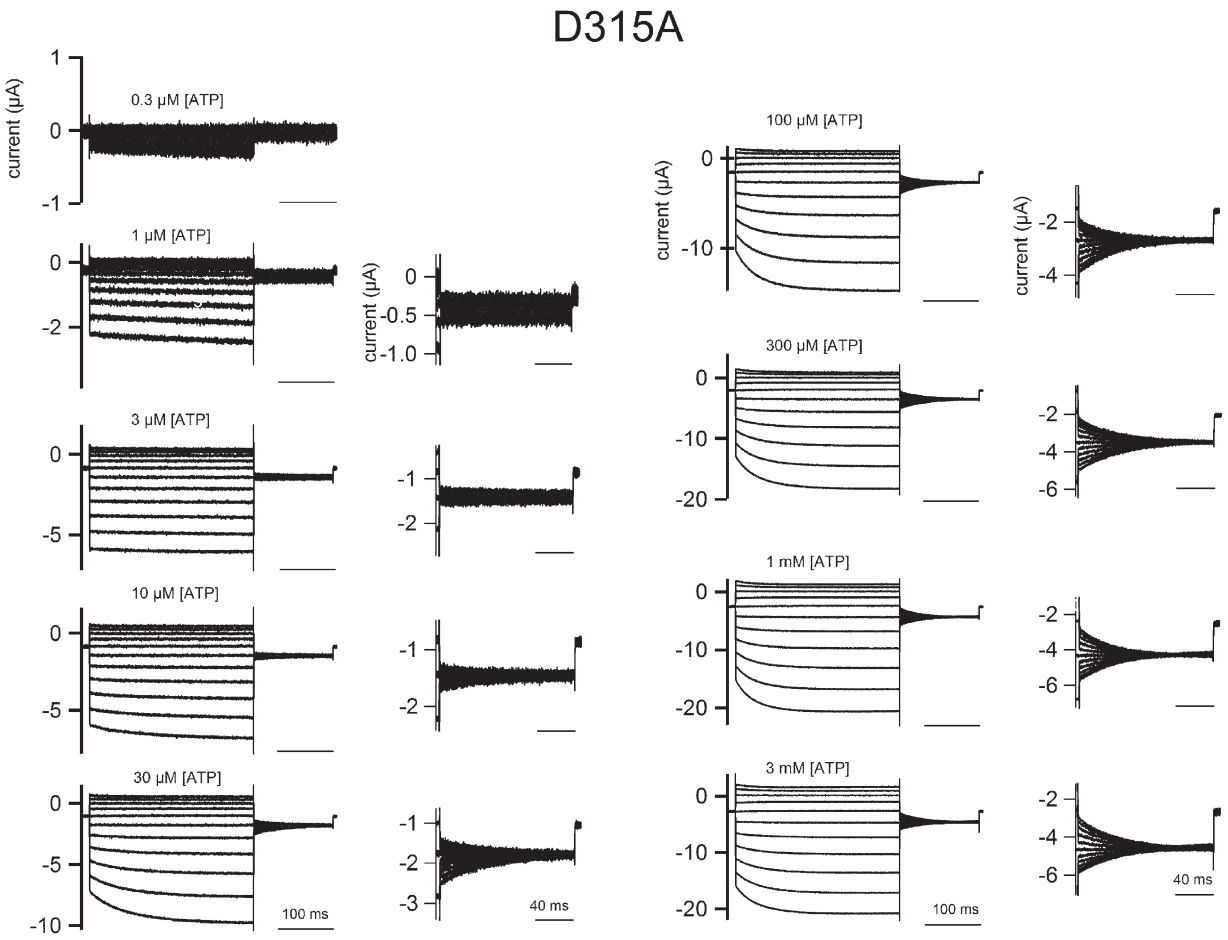

Figure S5. Representative macroscopic current recordings from D315A from a single oocyte, evoked by step pulses during the steady state after the application of various [ATP]. The holding potential was −40 mV. Step pulses from 40 to −160 mV were applied in 20-mV decrements. Tail currents were recorded at −60 mV, and their enlarged images are shown next to the main activation traces.

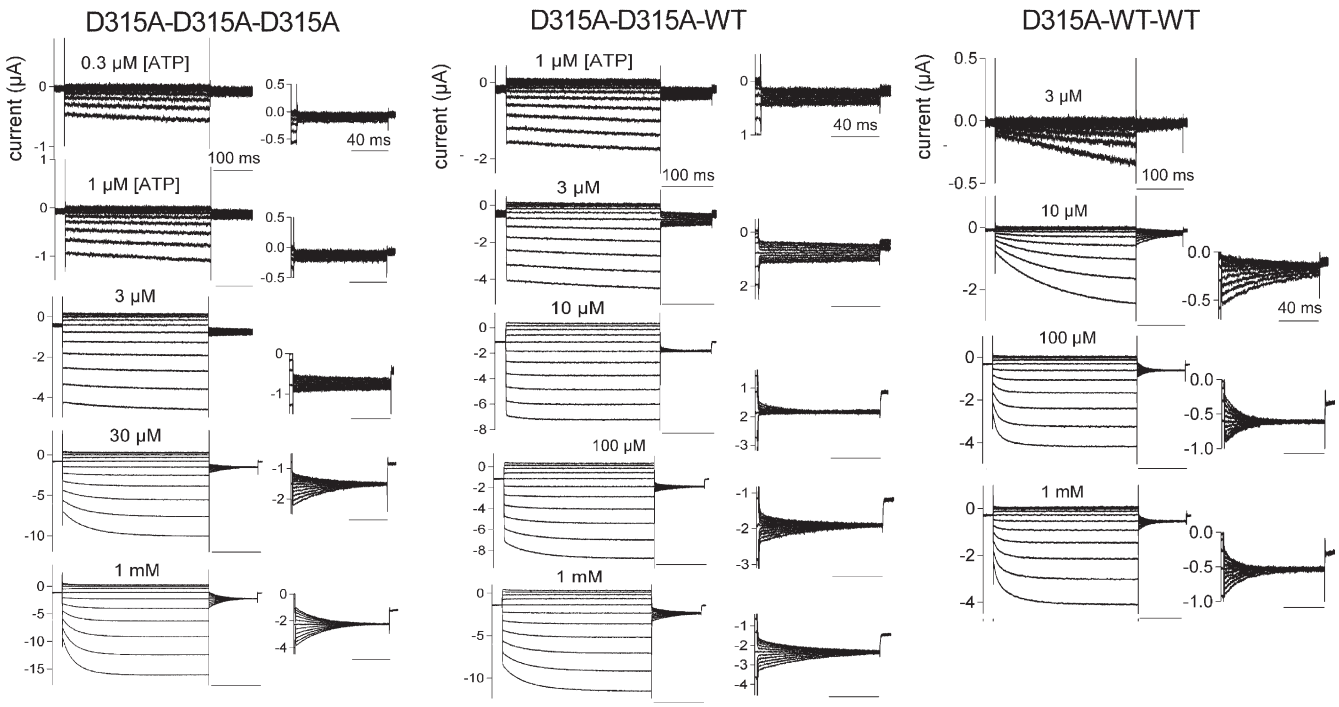

Figure S6. Representative macroscopic current recordings of tandem trimers with three, two, and one D315A mutant subunits. Responses were evoked by step pulses during steady state after the application of various [ATP] to the same oocyte. The holding potential was −40 mV. Step pulses from 40 to −160 mV were applied in 20-mV decrements. Tail currents were recorded at −60 mV, and their enlarged images are shown next to the main activation traces.

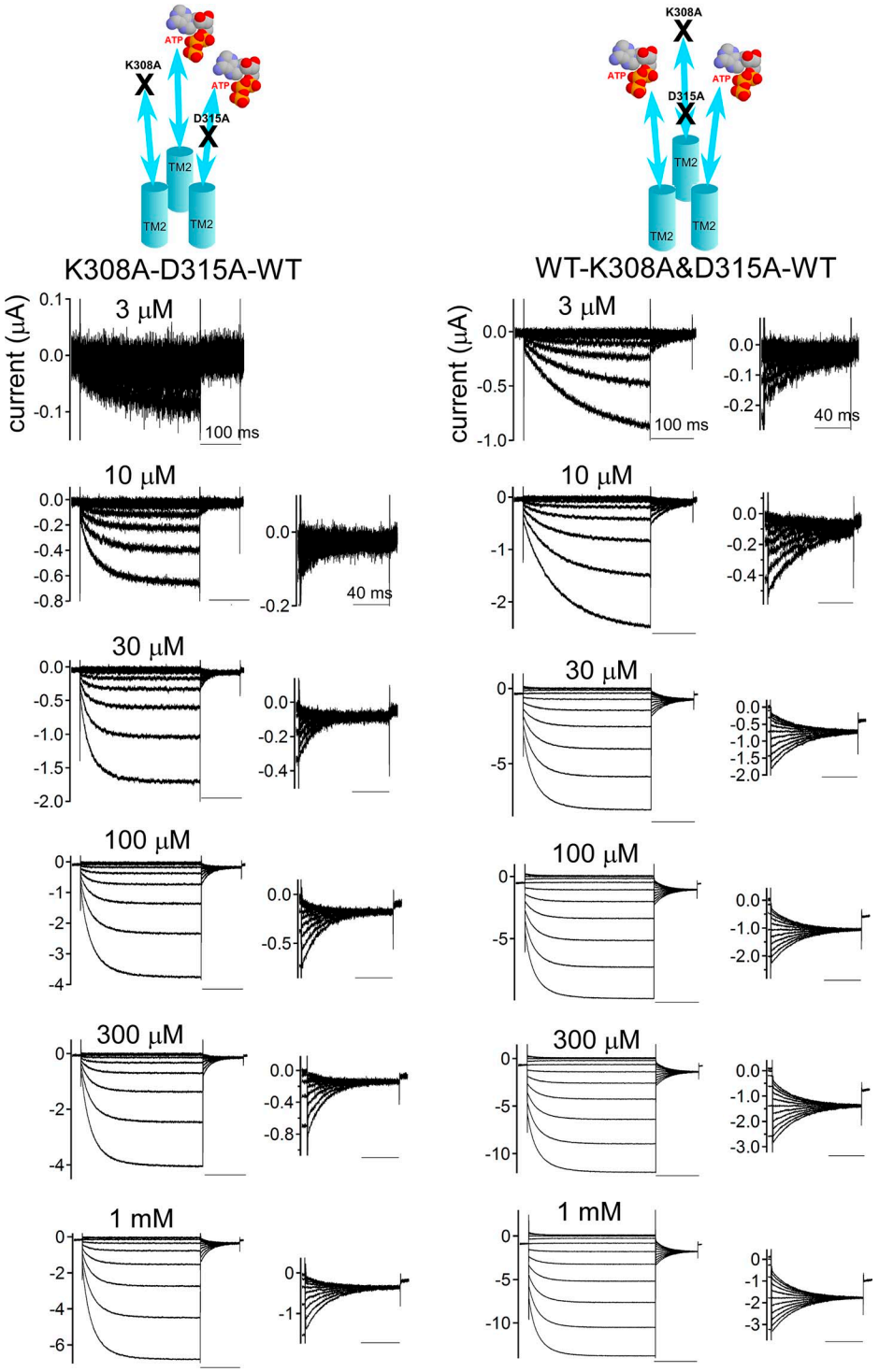

Figure S7. Representative macroscopic current recordings of *trans* (K308A–D315A–WT; left) and *cis* (WT–K308A&D315A–WT; right) tandem trimers. Responses were evoked by step pulses during the steady state after the application of various [ATP]. the holding potential was −40 mV. Step pulses are from 40 to −160 mV and were applied in 20-mV decrements. Tail currents were recorded at −60 mV, and their enlarged images are shown next to the main activation traces. Each set of recordings was obtained from a single oocyte.

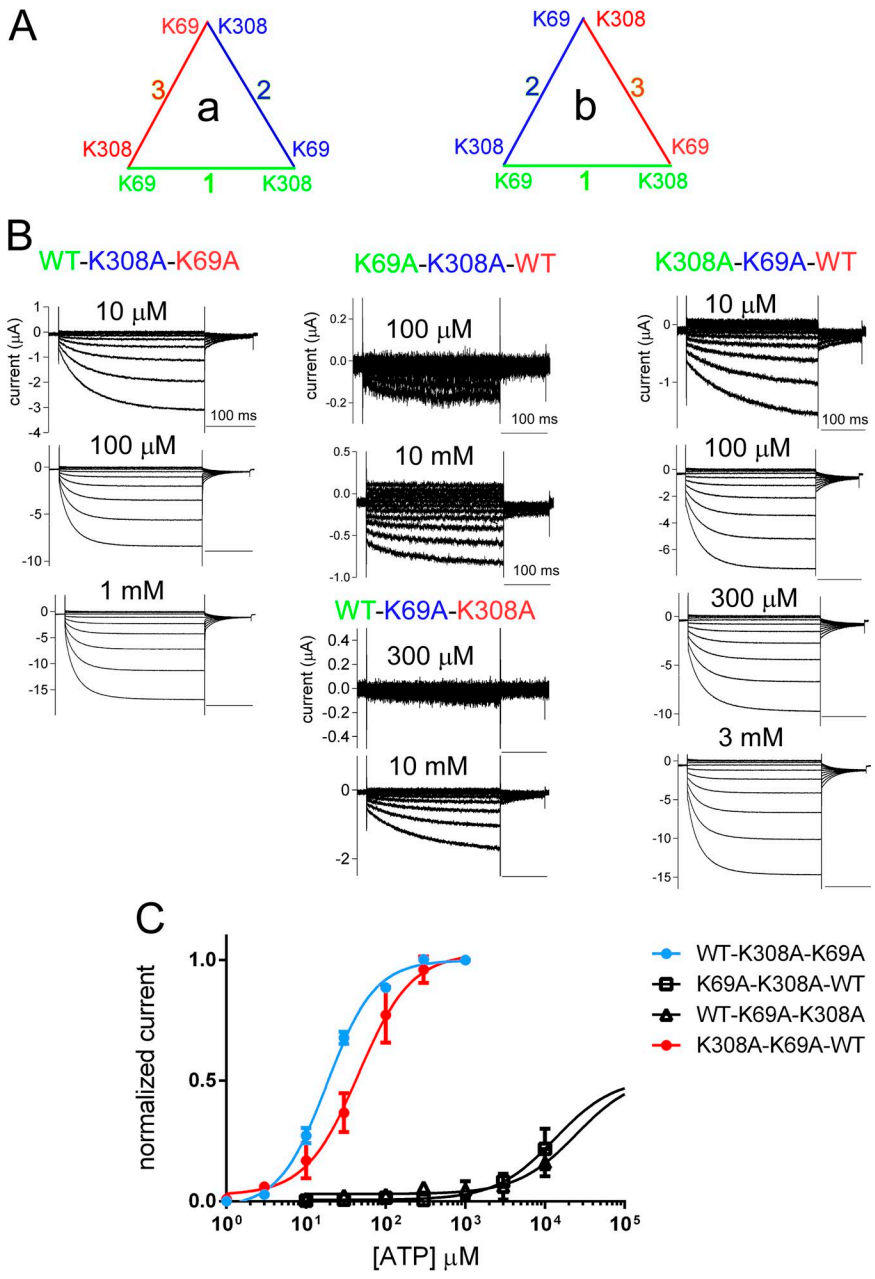

Figure S8. Analysis of the order of individual subunits in tandem trimers by using two different ATP-binding site mutations (K308A and K69A) simultaneously. (A) Schematic view of two possible arrangements of subunits in the trimer: a, counterclockwise; b, clockwise. Each subunit is represented by a different color. Each corner of the triangles represents one intersubunit ATP-binding site. (B) Representative traces for various constructs with two different ATP-binding block mutations, K308A and K69A. WT–K308A–K69A and K308A–K69A–WT show voltage- and ATP-dependent gating, whereas K69A–K308A–WT and WT–K69A–K308A hardly show any activation (n = 6). (C) [ATP] dose–response relationships of the TTCs used for subunit order experiments. Mean (± SEM) EC_{50} values for WT–K308A–K69A (n = 4) and K308A–K69A–WT (n = 5) are 18.3 ± 0.3 µM and 45.5 ± 1.8 µM, respectively. Hill coefficients for WT–K308A–K69A and K308A–K69A–WT are 1.5 ± 0.2 and 1.4 ± 0.2, respectively.

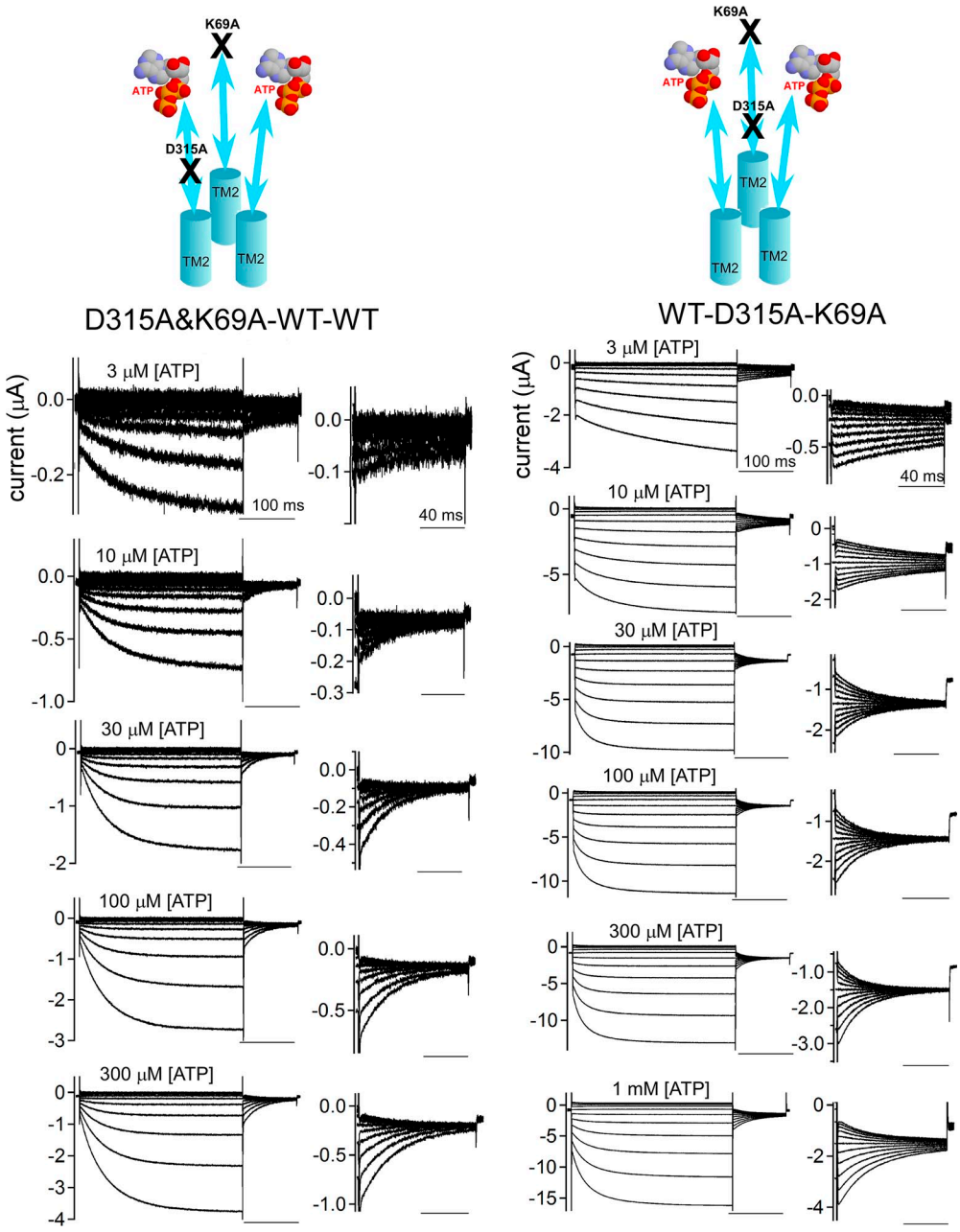

Figure S9. Representative macroscopic current recordings of D315A&K69A–WT–WT (left) and WT–D315A–K69A (right) evoked by step pulses in the steady state after the application of various [ATP]. The holding potential was −40 mV. Step pulses are from 40 to −160 mV and were applied in 20-mV decrements. Tail currents were recorded at −60 mV, and their enlarged images are shown next to the main activation traces. Each set of recordings was obtained from a single oocyte.

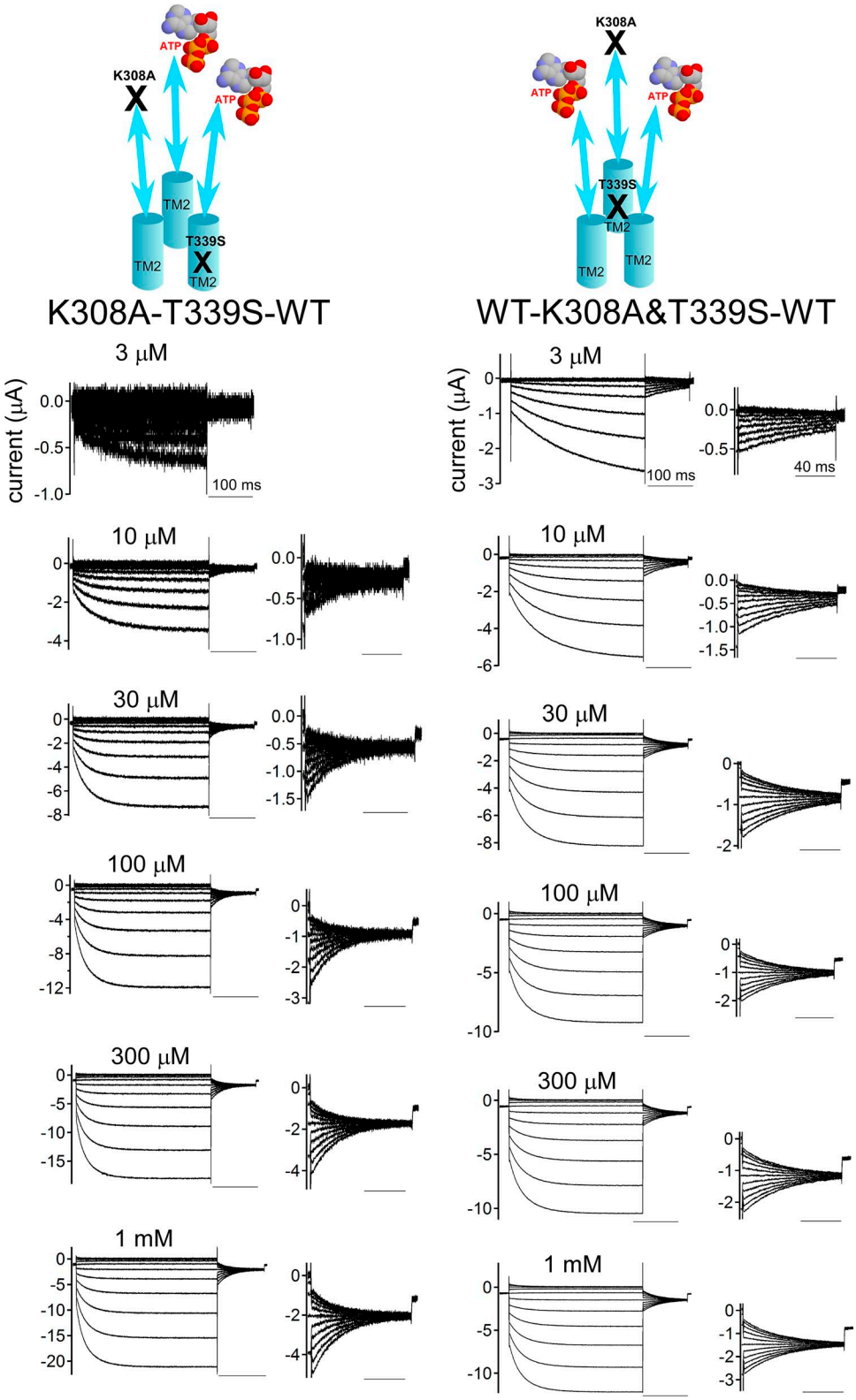

Figure S10. Representative macroscopic current recordings of *trans* (K308A–T339S–WT; left) and *cis* (WT–K308A&T339S–WT; right) evoked by step pulses during the steady state after the application of various [ATP]. The holding potential was −40 mV. Step pulses are from 40 to −160 mV and were applied in 20-mV decrements. Tail currents were recorded at −60 mV, and their enlarged images are shown next to the main activation traces. Each set of recordings was obtained from a single oocyte.

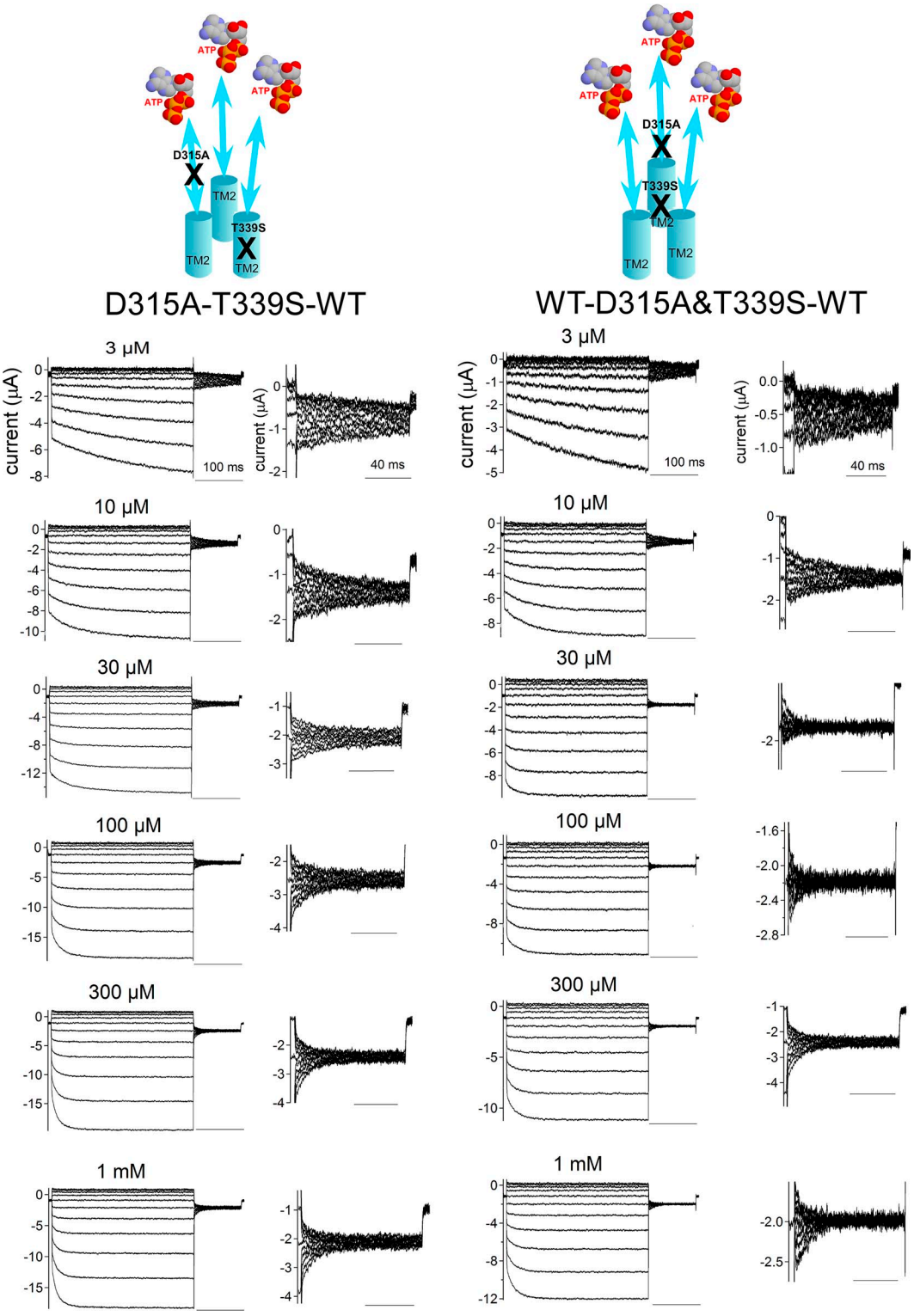

Figure S11. Representative macroscopic current recordings from *trans* (D315A–T339S–WT; left) and *cis* (WT–D315A&T339S–WT; right) evoked by step pulses during the steady state after the application of various [ATP]. The holding potential was −40 mV. Step pulses are from 40 to −160 mV and were applied in 20-mV decrements. Tail currents were recorded at −60 mV, and their enlarged images are shown next to the main activation traces. Each set of recordings was obtained from a single oocyte.

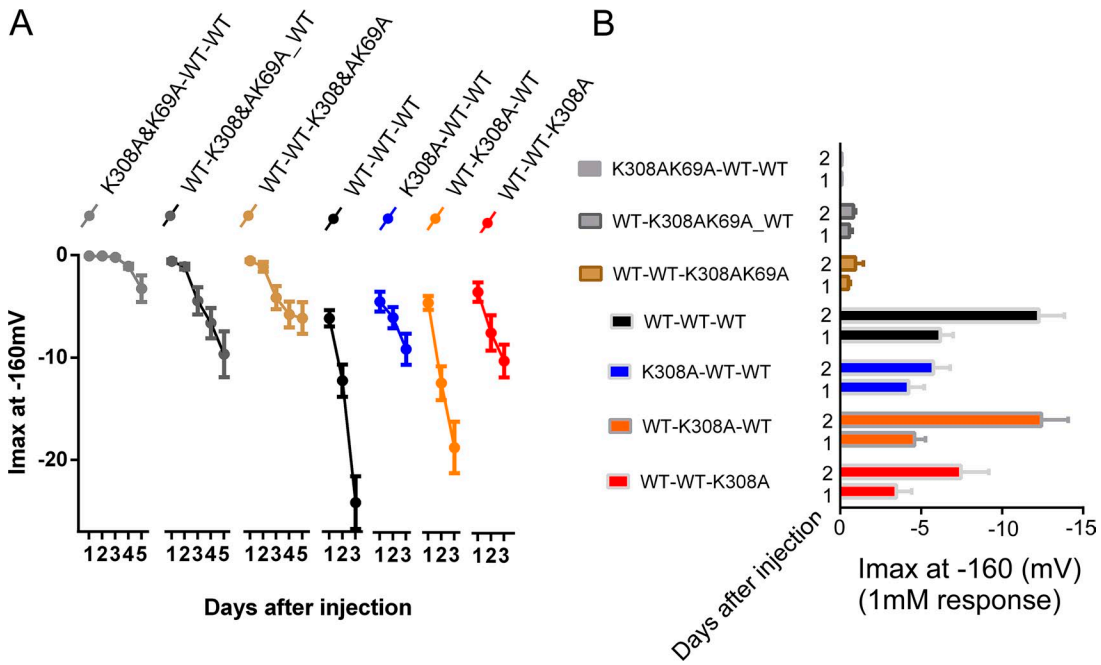

Figure S12. Analyses of the extent of possible hetero assembly between individual subunits of different TTCs. Any activation of the constructs (K308A&K69A–WT–WT, WT–K308A&K69A–WT, and WT–WT–K308A&K69A) is expected to indicate the presence of cross-assembly products of the WT subunits from different trimers, as two ATP-binding sites in the trimer are dysfunctional. (A) Cumulative data from two different batches of oocytes are shown. After injection of the same concentration of RNA (50 nl of 5 ng/µl), Imax at −160 mV was measured from the same oocyte on each day, and data were plotted as mean ± SEM (n values are between 18 and 28). (B) Cumulative data of Imax at −160 mV for the days 1 and 2, which corresponds to the time interval for the recordings performed in this study, are compared for all constructs and shown by bar graphs.

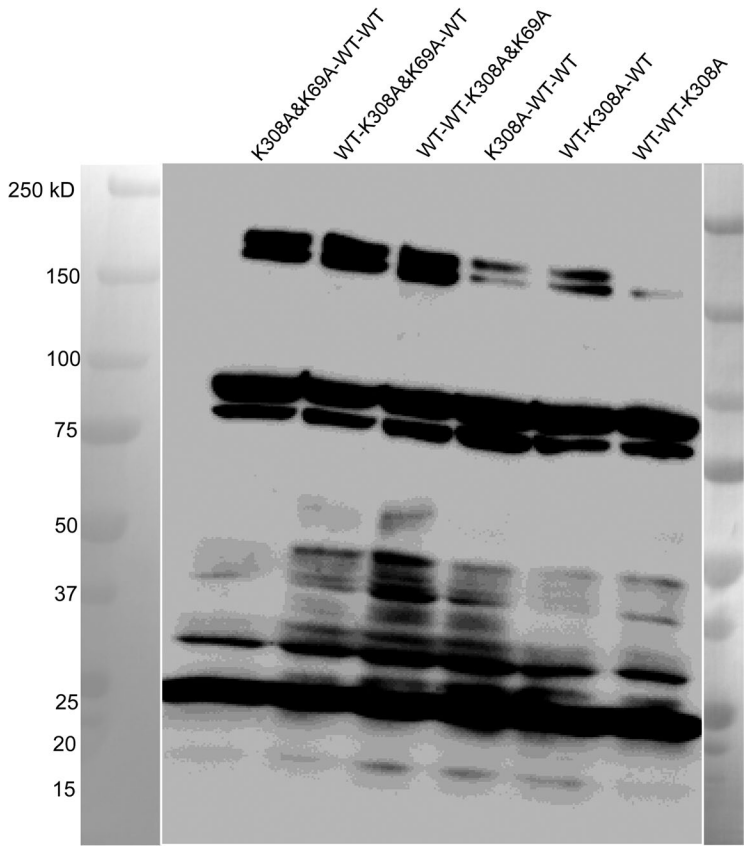

Figure S13. Western blotting of the constructs used for the analyses of the extent of possible hetero assembly in Fig. S12. Details of Western blotting are given in Materials and methods. White lines indicate that intervening lanes have been spliced out.

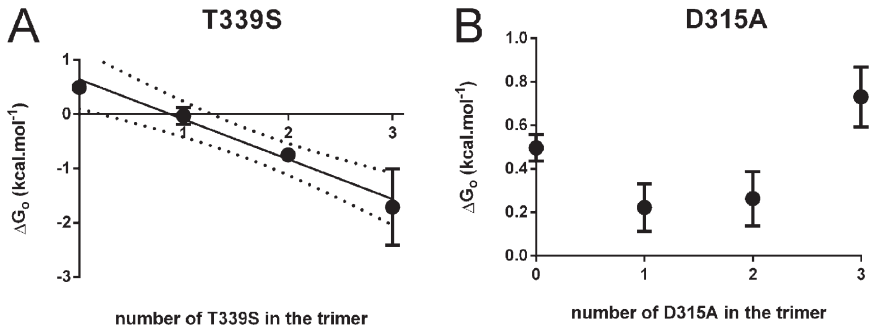

Figure S14. Free energy changes (ΔG, kcal/mol) versus the number of T339S or D315A mutations in the $P2X_2$ trimer. Free energy values at saturating concentrations of ATP at 0 mV for T339S (A) and D315A (B) mutants in the trimer (details of free energy calculations are given in Materials and methods). Free energy values for T339S could be well fitted by a straight line with slope of −0.74 (kcal/mol)/mutation (R^2 = 0.98). For D315A at the linker, there was no linear relationship between the free energy changes and the number of mutations.